Investigating Geologic and Rock Physics Controls on Acoustic Impedance of Deepwater Clastics – An Offshore West Africa Example

Obi Ifeanyichukwu S., Adegbaju T. Adetola, Akintayo O., Olopade A. Olabisi, and Adagbasa E. Goodluck
Esso Exploration and Production, Nigeria Limited, Lagos, Nigeria
Mobil Producing Nigeria Unlimited

ABSTRACT

Variations in reservoir acoustic impedance (AI) from low to high impedance relative to overburden shale can pose a significant challenge for seismic Interpreters aiming for consistency when mapping turbiditic boundary reflectors in a Deepwater field. In this study, an integrated evaluation of Miocene Deepwater (DW) slope channel complexes using well and quadrature phase broadband seismic data, showed that at shallow depths, most reservoir sands had lower acoustic impedance than shales but this flips to higher impedance at deeper intervals. The key objective of this work was to investigate possible impact of genetic DW facies, fluid, burial depth, and rock properties on observed relative acoustic impedance. Preliminary work includes generation of 30 well-to-seismic ties and 1D well synthetic models for selected wells for se in identifying key reflectors representing the base of individual complexes. Channel bases for the younger, low impedance reservoirs (SC1 – SC8) were mostly trough to peak zero-crossing while the older, higher impedance reservoirs (DC1 – DC6) were dominantly peak to trough zero crossing on quadrature phase data. Beyond the wells, 3D propagation of interpreted horizons was influenced by available seismic inversion volumes (Vsand and Phit). The next step featured comprehensive classification of the rocks into 7 genetic turbidite facies (R, S, Ta, Tb, Tc, Td, and Te/Sls/Slm) followed by detailed analysis of facies distribution within selected low and high impedance sands, and generation of cross plots of density, acoustic impedance, and compressional velocity with depth. The second phase of investigation was carrying out fluid substitution model analysis for AVO study and to evaluate possible impact of fluid type on acoustic impedance. The final exercise was generation of cross plots of Vp, Vp/Vs, Density, Por, and AI with depths for both sand and shales lithology. This was done to evaluate possible trends in the rock properties of sands and shales with depth. Our studies show that AI is primarily driven by Vp (rather than density). Most shallow reservoirs and gas sands are generally low impedance while the deeper reservoirs and oil/wet sands indicate higher impedance. Further screening show that sand intervals especially those of high impedance contain mainly traction/bedload and high concentration turbidites (R, S and Ta beds) while the shaly zones are mostly enriched in suspension or lower concentration turbidites (Td and Te/Sls/Slm). In summary, fluid fill and genetic DW lithofacies evaluation show minimal control on observed AI while burial depth (compaction) shows stronger impact on the reservoirs AI for this field.

Keywords: Deepwater, Turbidites, Channel Complex, Acoustic Impedance, AVO, VpVs, Den

INTRODUCTION

Acoustic impedance (AI) is the product of porous media density (Rho) through which a sound wave travels and the compressional velocity (Vp) of the sound wave (Andreassen *et al.,* 2007). For siliciclastic rocks, the strength of impedance contrast between sand and shale rocks is a key determinant of the seismic reflector character as well as the ease of interpretation by subsurface interpreters. Variations in reservoir acoustic impedance (AI) from low to high impedance relative to overburden shale can pose significant challenges for seismic interpreters considering that AI typically helps in categorizing sands from shales. Al-Khazraji *et al* (2018) utilized acoustic impedance inversion to discriminate between sand and shale facies. In this study, detailed interpretation of Deepwater slope channel complexes using well, and quad phase broadband seismic data showed that reservoir sands have lower AI than surrounding and overburden shales at shallow depths but flip to higher impedance at deeper sections. Similar observations were made by Al-Khazraji *et al* (2018) who noted that in a vertical sense, AI [of reservoir sands] increased with depth, while laterally decreased with decreased sand content and increased shale content. To better understand these behaviors, we made efforts to evaluate some geological and rock

The authors wish to thank NNPC Limited, NNPC Upstream Investment Management Services (NUIMS), Esso Exploration and Production Nigeria Limited (EEPNL), and Shell Nigeria Exploration and Production Company (SNEPCO) for release of the materials and permission to publish this work. Many thanks to the Geoscience community of the EEPNL for technical reviews and suggestions.

physics factors that could influence observed AI trends in this field.

Depositional and diagenetic changes are two key geologic elements that impact both sands and shales as they become progressively buried. In Avseth *et al* (2008), depositional trends in marine shales have been associated with distance of the rock from the coastline. Such trend has also been tied to variation in silt content and certain types of clay minerals. For deep-marine siliciclastic systems, as burial progresses, smectite-rich shales typically undergo illitization and loss of bound water, causing both a porosity reduction and mineralogy change. When buried up to ~2 km depth, both sands and shales are exposed mainly to mechanical compaction (Storvoll et al., 2005; Avseth et al. 2008). At the transition zone (70-80°C), two concurrent chemical processes and a change from mechanical to chemical compaction occurs for sand-shale sequences. Smectite to illite (and possibly chlorite) transformation in the shales, as well as quartz cementation of sandstones. The chemical alteration of the shales could generate cements which serve as initial cementation agent for quartz and other grain content of the sands (Avseth et al 2008). This mineral alteration is seen in marine shales all over the world (Bjørlykke, 1998).

GEOLOGIC FRAMEWORK

This study was carried out on deepwater slope confined channel complexes located in the Niger Delta Basin offshore Africa (Fig. 1) at about 1200m water depth. It is a brown field asset with over 20 production wells and several water and gas injection wells. The field is set-up by a large regional detachment fold which is positioned in the boundary between a coupled extensional – contractional system (Fig. 2). Early development drilling demonstrated the presence of locally sealing shales especially at the deeper intervals.

The Niger Delta basin is primarily a linked extensional - compressional tectonic system with distinct structural provinces (Corredor *et al.* 2005). Updip, extension at the shelf margin is composed of landward dipping growth faults and basinward dipping normal faults. Downdip and along slope, is dominantly compressional, composed of large mobile shale cored folds, followed by smaller scale buckle folds, and finally ends in belts of low relief toe-thrusts. This system is driven by gravitational collapse of a prograding deltaic sediment wedge that prograded along with the sediment wedge (Corredor *et al.,* 2005; Obi et al., 2018). In this study region, there are three phases of associated depositional and structural history. The first was an early phase of deposition and associated mini-basin development at ~35 ma. This was followed by contraction expressed as buckle folding linked to up-dip extension at ~20 ma. Finally, as the depositional systems prograded, the location of extension migrated basinwards. The geologic column in the Tertiary Niger Delta is subdivided into three lithostratigraphic formations namely the marine Akata Formation, paralic Agbada and continental Benin Formation (Avbovbo, 1978). Deepwater reservoirs in this area are primarily in the Agbada formation.

In terms of stratigraphic framework, two distinct fairways have been interpreted in this field representing 2nd order hierarchical packages called the Upper and Lower fairways (Fig. 3a). The Lower fairway is comprised of 6 channel complexes (DC1 – DC6), while the Upper fairway contains 8 channel complexes (SC1 – SC8). Both fairways have different vectors (Fig. 3b). In the Lower fairway, simultaneous erosion (creation of valleys) as well as deposition of deep-water strata were the earliest phase of activity in the area. Collapse and rotation of unstable deposits in the form of slump deposits in a progressively developing canyon created the DC1. This was followed by deposition of bedload deposits in space-constrained areas of the canyon (DC2) and meandering channel systems within confined to weakly confined settings (DC3 and DC4). The DC3 shows evidence of lateral channel migration as indicated by the presence of lateral accretion packages (LAPS) typical of more sinuous channel systems (Abreu et al., 2003). The DC4 on the other hand is weakly confined with evidence of sand waves and levees both within the channel thalweg and in the off-axis areas. The DC5 and DC6 are levee confined channel complexes with high amounts of preserved internal levees and channel margin facies (Fig. 3a). This channel complex set is capped by a major re-incision which marks the top of the lower fairway as well as the beginning of the upper fairway. The Upper fairway, at early stages, featured periodic changes in depocenter location as the main control for repeated switch in position of the individual channel complexes for the first set of erosionally confined complexes (SC1 – SC4) (Fig. 3). Each time there is a new surge of sediment supply, the new deposits take advantage of adjacent available depositional low (considering the depositional inner bank and erosive outer bank of the preceding cycle), eroding parts of the pre-existing underlying channel complex and placing its sediments in the new location (Oomkens 1967, 1974). The process continues and is repeated when the current depocenter builds elevation there by creating an adjacent depositional low for the new cycle of deposits to occupy. According to Obi and Mode (2011), gradual reduction in the overall depositional energy with increased accommodation results in smaller, higher sinuosity, levee confined complexes such as SC5 – SC8 with more preserved internal and external margin facies (Fig. 3a).

DATA AND METHODOLOGY

The Puzzle: Why Varying Acoustic Impedance? Our Data and Observations

A total of 14 channel complexes from 30 wells were evaluated to better understand the rock physics and

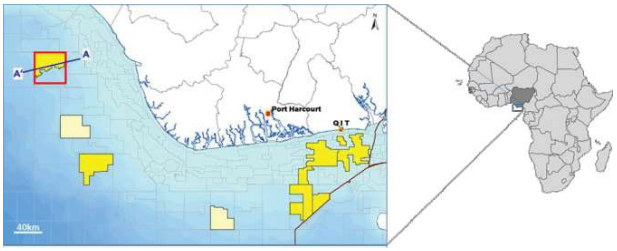

Figure 1: Acreages in the Niger Delta Basin showing study field study location in Red box.

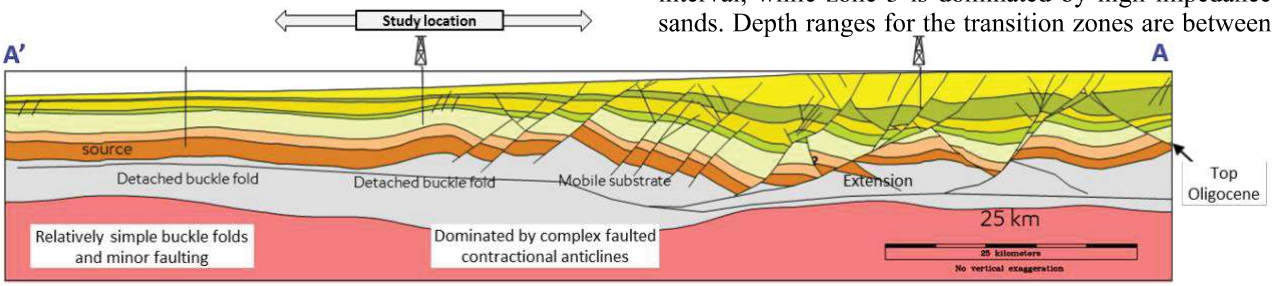

Figure 2: Sub-regional transect showing structural provinces (coupled extensional – compressional system). Study location \ sits on a detachment fold in central portion of asset (Courtesy ExxonMobil Deepwater Collaborative 1999).

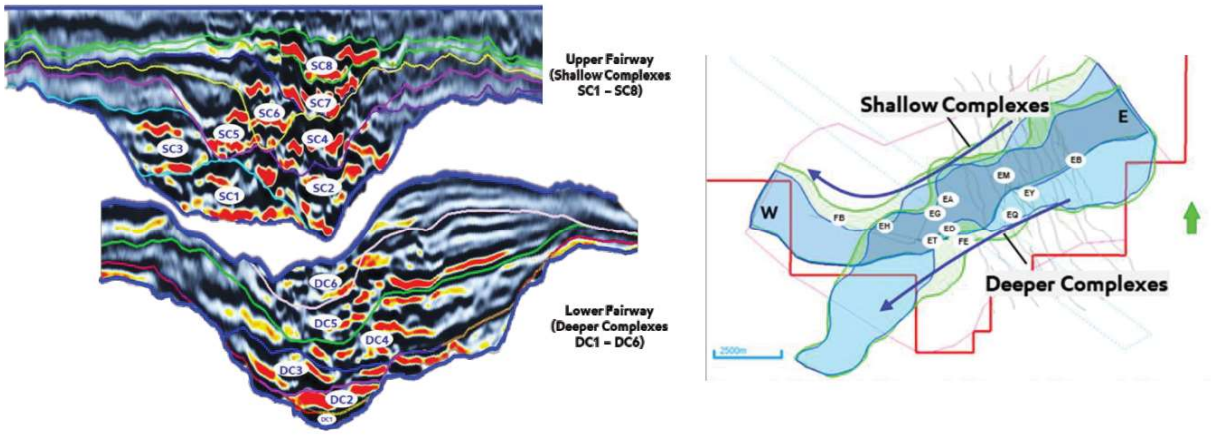

Figure 3a: Stratigraphic framework and depositional sequence of study area. Note different vectors for the Upper and Lower Fairways in figure 3b.

possible controls on the acoustic impedance of individual reservoirs. A key observation is that there is a mix of both high and low acoustic impedance reservoirs mostly in the vertical sense (Table 1). Although the transition zones are not quite clear, the shallow channel complexes (SC1-8) have mostly lower impedance reservoirs while the deeper complexes (DC1-6) were mostly high impedance. Lower impedance in this context means that the sands have low acoustic impedance than the surrounding shales with high impedance and vice versa. From the summary shown in table 1, 3 main zones were identified. In zone 1 (SC3 – SC8), 105 out of 116 penetrations (90.5% of the population) are low impedance sands, 10 of them (8.6%) had low impedance contrast and difficult to classify as high or low impedance sands, while the remaining penetration (0.8% of the population) was high impedance. The middle zone (SC1 and SC2) is a transition interval containing both low and high impedance sands. Of the 36 individual well penetrations, 15 of them (42%) are low impedance, 8 of the population (22%) are sands with low impedance contrast, while the remaining 13 (36%) are high impedance. In zone 3 (DC1 – DC6), 4 out of the 42 penetrations (7.1%) were low impedance, 1 had low impedance contrast, while the remaining 38 (90.4%) were high impedance. Summarily, zone 1 is comprised mainly of low impedance sands, zone 2 is mixed or transition interval, while zone 3 is dominated by high impedance sands. Depth ranges for the transition zones are between 3100 and 3550 m SSTVD. We carried out integrated turbidite facies evaluation, cross plots analysis of key rock physics parameters, fluid substitution modeling and other rock physics study for better understanding of possible impact of facies, fluid, lithology, or depth on observed acoustic impedance trends.

RESULTS AND DISCUSSION

Acoustic Impedance vs Genetic Turbidite Facies

Seven genetic turbidite beds were defined using core-log relationships to group the rocks into petrofacies (Fig. 4). An integration is also made between the Bouma sequence of 1962 (low energy turbidite sequence represented by Ta, Tb, Tc, Td and Te beds) and the Lowe sequence of 1982

Table 1: Well data showing observed reservoir acoustic impedance distribution relative to overlying shale. Compare reservoir impedance matrix for both shallow and deep channel complexes.

		Shallow Channel Complex								Deep Channel Complex					
		Zone 1						Zone 2		Zone 3					
Fault Block	**Wells**	**SC8**	**SC7**	**SC6**	**SC5**	**SC4**	**SC3**	**SC2**	**SC1**	**DC6**	**DC5**	**DC4**	**DC3**	**DC2**	**DC1**
CFB	EM	Y	Y	Y	Y			Y	Y						
CFB	ES	Y		Y	Y		Y								
CFB	EV	Y	Y	Y	Y	Y			Y		Y	Y	Y		
CFB	EZ	Y	Y		Y		Y								
CFB	FC	Y	Y		Y		Y								
EFB	EB	Y	Y	Y		Y		Y		Y	Y	Y	Y		
EFB	EW	Y	Y	Y	Y	Y		Y							
EFB	EY	Y	Y			Y		Y	Y			Y			
EFB	FD	Y	Y	Y	Y				Y	Y					
EFB	EC	Y	Y	Y	Y	Y		Y		Y	Y	Y			
WFB	FE	Y	Y	Y		Y		Y	Y	Y		Y			
WFB	EH	Y		Y	Y	Y									
WFB	EI	Y	Y	Y	Y	Y			Y						
WFB	EJ	Y	Y	Y	Y		Y								
WFB	EK	Y	Y	Y	Y	Y			Y	Y	Y	Y	Y		
WFB	EL	Y	Y	Y		Y		Y	Y		Y	Y			
WFB	FF	Y	Y	Y		Y		Y	Y						
WFB	EN	Y	Y	Y		Y		Y	Y						
WFB	EO	Y	Y	Y		Y		Y	Y		Y	Y			
WFB	EP	Y	Y	Y	Y				Y			Y			
WFB	EQ	Y	Y			Y		Y		Y	Y				
WFB	EA	Y	Y	Y	Y			Y	Y	Y	Y	Y	Y		
WFB	ER	Y	Y	Y	Y			Y	Y		Y				
WFB	ET	Y	Y		Y	Y		Y	Y		Y	Y			
WFB	EU	Y	Y		Y	Y			Y		Y				
WFB	FA	Y	Y		Y	Y			Y		Y				
WFB	FB	Y	Y	Y	Y										
WFB	ED	Y	Y		Y	Y		Y	Y		Y	Y			
WFB	EE	Y	Y	Y	Y	Y		Y	Y		Y				
WFB	EF	Y	Y	Y	Y	Y		Y	Y		Y	Y		Y	
WFB	EG	Y		Y	Y	Y		Y	Y		Y	Y	Y		

Key

Y Interval present (Low Impedance)
Y Interval present (Low Contrast)
Y Interval present (High Impedance)

(high energy turbidite sequence represented by the R and S beds). The Rbeds are coarse grained units with >30% gravel content while S-beds contain 5-30% gravel content. The sandy beds are subdivided into 3 types- Ta, Tb and Tc beds. Ta beds are massive to normally graded coarse to fine-grained sands. Tb are parallel laminated sandstones while Tc are current rippled sands. Td beds are parallel laminated siltstones while Te are laminated to massive mudstones. We used poro-perm plots and core interpretation from 5 wells to generate transforms representing rocks groups, namely High concentration turbidites (HCTs), Low concentration turbidites (LCTs), Very Low concentration turbidites (VLCTs) and non-net facies. The first transform also called the HCT is comprised mainly of bedload and traction facies namely R, S, Ta and Tb beds. The LCTs (Transform 2) is dominated by Tc beds, while the VLCT (Transform 3) are mainly Td beds. The Te and other slump and debritic beds which make up one end member of the VLCT are classified as non-net. In this grouping, the best reservoirs are R, S, Ta, Tb and Tc beds while the poorest reservoirs are those containing Td and Te beds. With regards to the

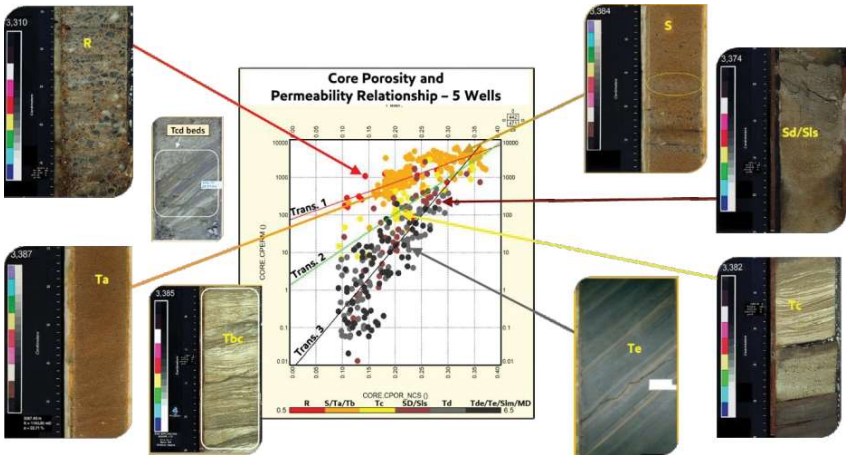

Figure 4: Core Poro-Perm plot from selected wells showing both Bouma and Lowes facies. Also note all 3 transforms and clustering of individual turbidite facies.

individual turbidites (Fig. 5 and 6), the sandy rocks contain mostly R, S and Ta beds while the shaly rocks are dominated by Td and Te beds. On the acoustic impedance column of Figure 6, both low and high acoustic impedance sands were present. A closer look at the genetic content of individual sands showing either high and low acoustic impedance, it is observed that they both contain similar turbidite facies, mostly R, S, Ta and Tb beds (Fig. 6). However, there is concentration of bedload R and S beds in the high impedance sands.

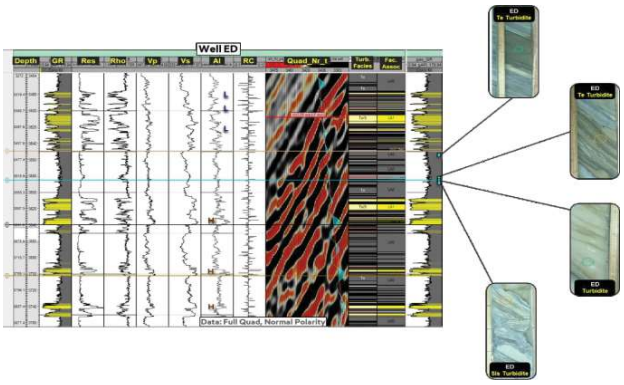

Figure 5: Well EB seismic-well tie with cored intervals. Observe high acoustic impedance for most reservoirs and dominance of R, S and Ta/Tb turbidite facies in those sands. (Note: **H** = High AI sands).

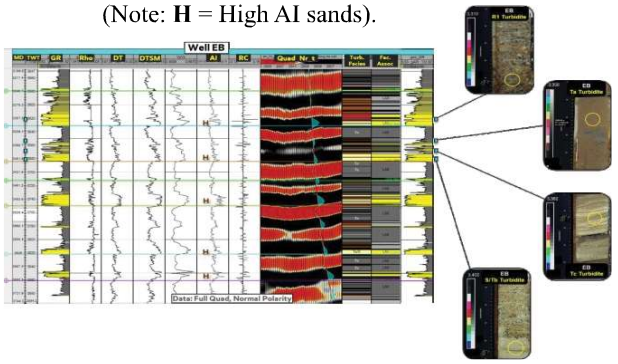

Figure 6: Well ED seismic-well tie with cored intervals. Observe similar occurrence of S and Ta/Tb turbidites in both high and low impedance sands. (Note: **L** = Low AI sands; **H** = High AI sands).

Cross plots of bulk density, compressional velocity (Vp) and acoustic impedance with depths were generated for the different turbidite sand beds. In the plots of bulk density against depth, sands containing high concentration Ta and Tb turbidites had lower density than those dominated by suspension turbidites namely Td and Te beds (Fig. 7). Some wells show overlaps between clusters of high and low concentration turbidites, but the general observation of acoustic impedance distribution is the same. No clear trend was noticed for the R and S beds even though they mostly track the Te beds especially at deeper intervals. Despite overlaps in some wells, the cross plot of Vp vs depth from most wells show that sands containing mostly Td and Te beds have lower Vp range while R, S and Ta dominated sands are in the higher Vp spectrum (Fig. 8). The acoustic impedance versus depth plot for individual turbidites show that at shallow depths, there is significant overlap between Ta, Tb- dominated sands and Td, Te dominated sands (Fig. 9). At deeper intervals, both Td and Te beds have lower impedance than Ta, R and S beds. In wells FE, at shallow depths, the Ta turbidities have lower acoustic impedance than Td and Te beds, but the trend flips at deeper depths (Fig. 9). In all cases made, there is greater separation between end members of the turbidite facies at deeper intervals.

Reservoir Fluid Types and Acoustic Impedance

1D Seismic modeling was carried out for selected wells to understand the AVO response of the rocks at different fluid content scenarios. For this paper, we have used displays from one wet and one hydrocarbon bearing well to show the AVO observations at different fluid cases. For siliciclastic reservoirs, rock physics and AVO depth trends can be very complicated depending on mineralogy, lithology, diagenesis, pore pressure, effective stress, and fluid properties (Avseth *et al* 2003). For a better understanding of expected seismic response at any depth, it is important to consider expected contrasts in the elastic properties of sands vs shales at any such depth. Brown and Abriel (2014) showed the expected AI trend for hydrocarbon-bearing sand, water-bearing sands, and shales in same basin. Their plot shows that bright spots are expected at shallow depths where sandy rocks generally have lower AI than surrounding shales, while dim spots are expected at deeper intervals below the depth where polarity reversal occurs (Fig. 14).

In the western area of the field, hydrocarbon bearing well ED (Fig. 10) show shallow sands SC6 and SC8 with low acoustic impedance while the deeper DC1, SC1 and SC4 show higher acoustic impedance. So, these hydrocarbon sands have generally low acoustic impedance at shallow depths but become high impedance at deeper intervals. In terms of AVO, there is a general decrease in amplitude with offset irrespective of depth or whether sand contains oil, gas, or brine. Several sands showed Class 2P AVO response with the polarity reversal occurring at progressively lower angle between in situ and gas fluid contents (Fig. 10). In terms of reflector character, keeping in mind that this synthetic model was generated using normal polarity quadrature seismic data, sand bodies with low acoustic impedance (SC6 and SC8) correspond to a synthetic trough while the base of sands corresponds to trough to peak zero crossing. Sand bodies with high acoustic impedance (DC6, SC1 and SC4) corresponds to a synthetic peak with the bottom boundary matching with the peak to trough zero crossing. The AVO inset shown is tied to the red and blue lines within the SC4 sand.

Well EB in the east area of the field (Fig. 11) containing wet reservoirs was subjected to similar fluid substitution

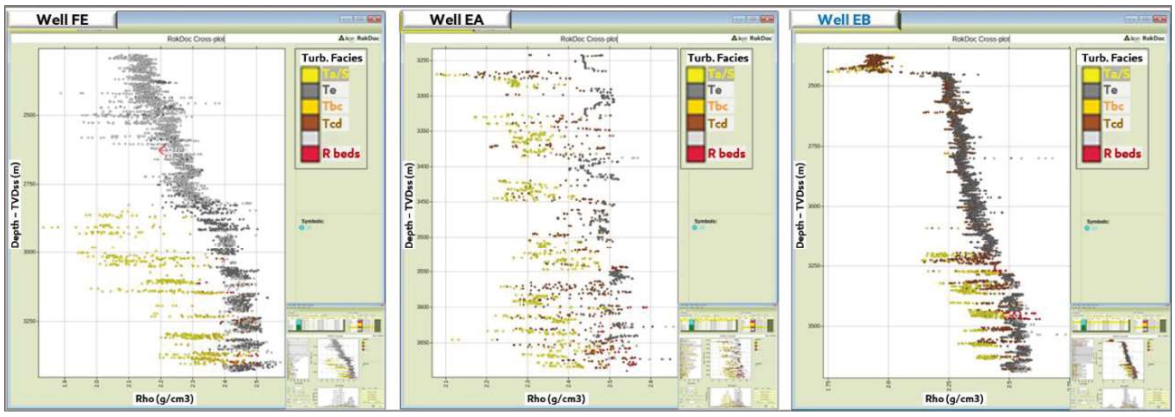

Figure 7: Rho vs Depth plot for wells FE, EA and EB. Note that sands containing mostly Ta and Tb turbidites have lower density than those dominated by Td and Te turbidites.

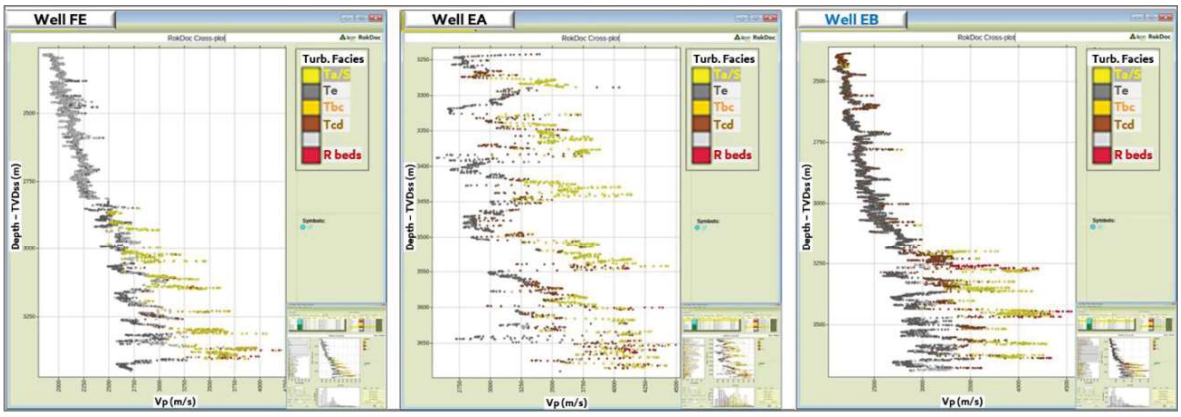

Figure 8: Cross plot of Vp vs depth from most wells showing that sands containing mostly Td and Te beds have lower Vp range relative to R, S and Ta dominated sands.

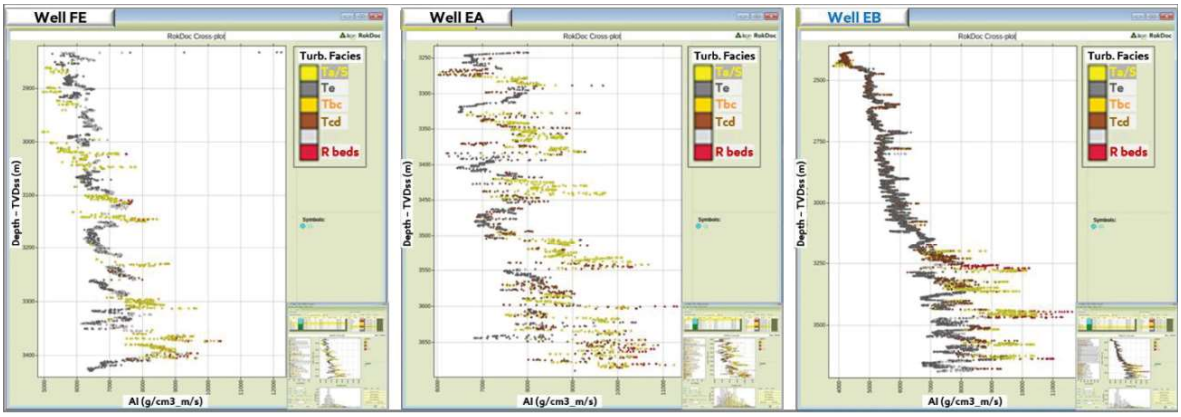

Figure 9: Cross plot of AI vs depth. Note overlap between Ta, Tb- dominated sands and Td, Te dominated sands at shallow depths. Both Td and Te beds have lower impedance than Ta, R and S beds at deeper depths.

exercise. For this well, both shallow and deep sands show high acoustic impedance, and the sand body ties to a synthetic peak. In similar manner to well ED, there is reduction in amplitude with offset with a same 2P response for both insitu, oil and gas fluid scenarios. It is also noted that amplitude flips from positive to negative values occur at progressively lower angles between the insitu and gas fluid cases. Summarily, we note that irrespective of fluid type (gas, oil or brine), the acoustic impedance of the sands (relative to shale) is not driven by fluid type as both high and low impedance sands show similar response in different fluid cases.

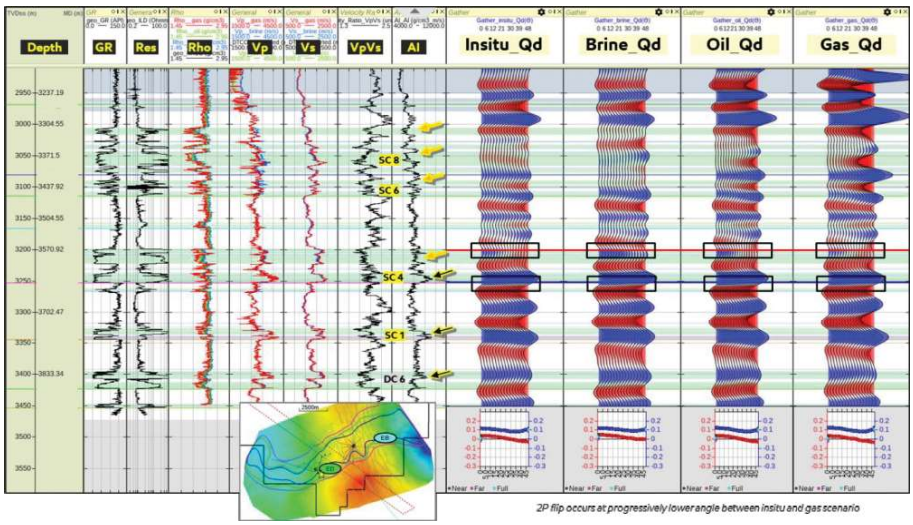

Figure 10: Well ED (hydrocarbon bearing) seismic and fluid substitution (AVO plot taken from red and blue lines in black boxes).

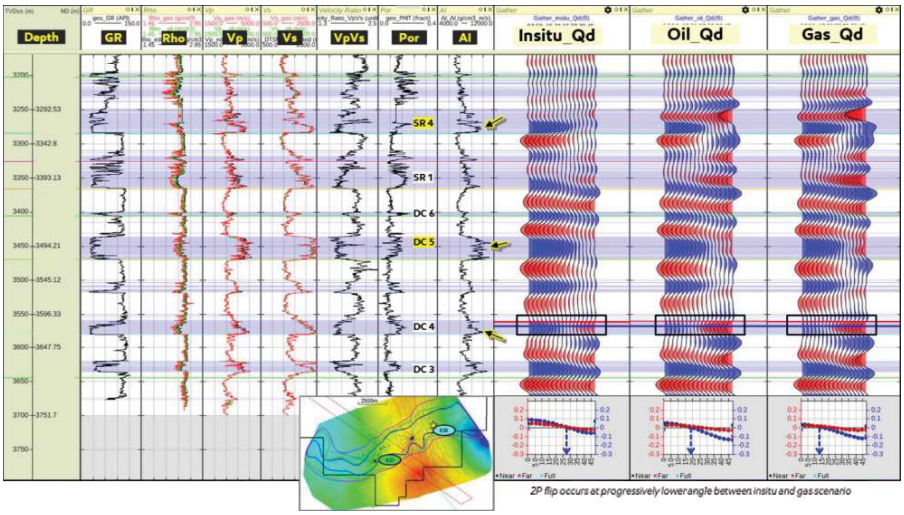

Figure 11: Well EB (wet) seismic and fluid substitution model (AVO plot taken from red and blue lines in black boxes).

Sand and Shale Vp, Vp/Vs, Den, Porosity and AI trends with Depth

Acoustic impedance of individual sand and shale lithologies was plotted against depth to investigate possible trends for each rock type. Cross plots of density, porosity, Vp and Vp/Vs with depth were also generated for the sands and shales. In the integrated plots, density, acoustic impedance, and compressional velocity (Vp) increases with depth for both sand and shale lithologies (Fig. 12a, 12b and 12d). On the acoustic impedance vs depth plot (Fig. 12b and 13), the generalized plot shows some sands with lower AI than the overburden shales at the shallow depths, but transitions to higher impedance at deeper intervals. In other words, the compaction trend is not uniform for both sands and shales hence the flip in acoustic impedance. According to Brown and Abriel (2014), hydrocarbon-filled sand, water-filled sands, and shales in same basin have different compaction trends with sands starting off as lower AI at shallow depths and then crossing over to higher AI values at deep intervals. In terms of direct hydrocarbon indicator in seismic sections, figure 14 shows polarity reversals represented in AI vs depth and age plot, where bright spots are the observed seismic phenomena for prospective reservoirs above the crossover zone, while dim spots are detected for reservoirs below the cross-over zone (Brown and Abriel, 2014).

Compressional velocities (Vp) and densities of siliciclastic sedimentary rocks display increase with depth due to compaction and porosity reduction (Avseth *et al*

2003). Although porosity, as expected, decreases with depth, sandy rocks show higher range of average porosities than the shaly rocks (Fig. 12c). At deposition, shales tend to have relatively high porosities compared to sands. Sands will have depositional porosities of approximately 0.4, while shales can have depositional porosities of more than 0.8. Heterolithics can have even lower depositional porosity than 0.4, as clay particles will fill the pore space of the sand frame (Avseth *et al,* 2003).

As burial proceeds, porosity reduces as changes occur due to grain packing and ductile deformation (Fig. 18). However, shales show faster compaction than sands, causing a crossover of the porosity-depth trends of sands and shales (Fig. 12c, 14 and 18). At greater depths, different diagenetic processes occur. Sands lose porosity mainly due to cementation, while shales lose intrinsic porosity as bound water is released (Avseth *et al* 2003).

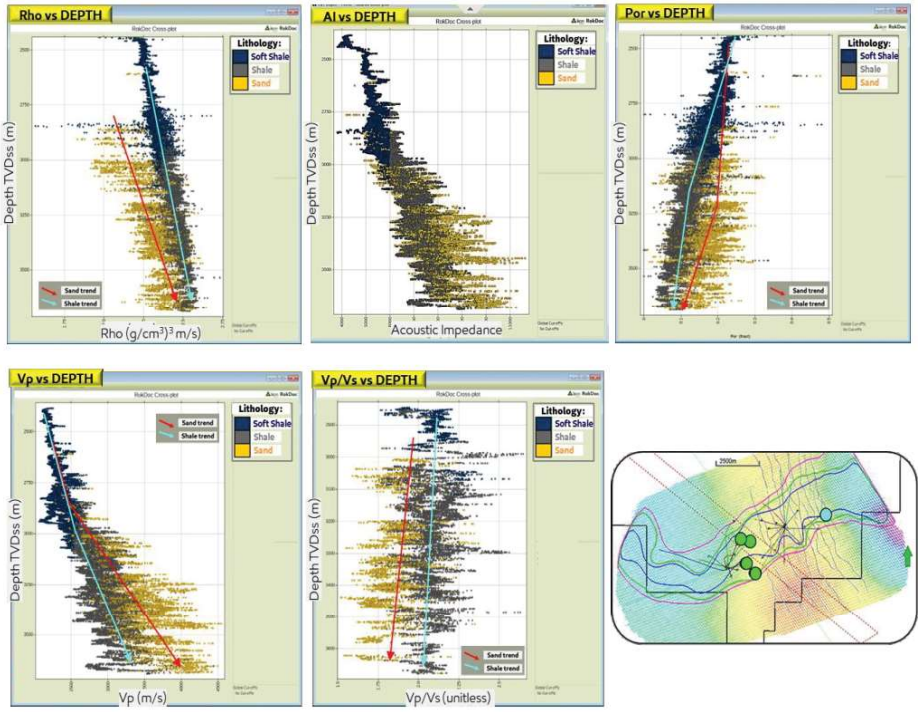

Figure 12: (a) Density, (b.) Acoustic Impedance (AI), (c.) Porosity, (d.) Compressional velocity (Vp), and (e.) Vp/Vs, versus depth plot (5 wells)

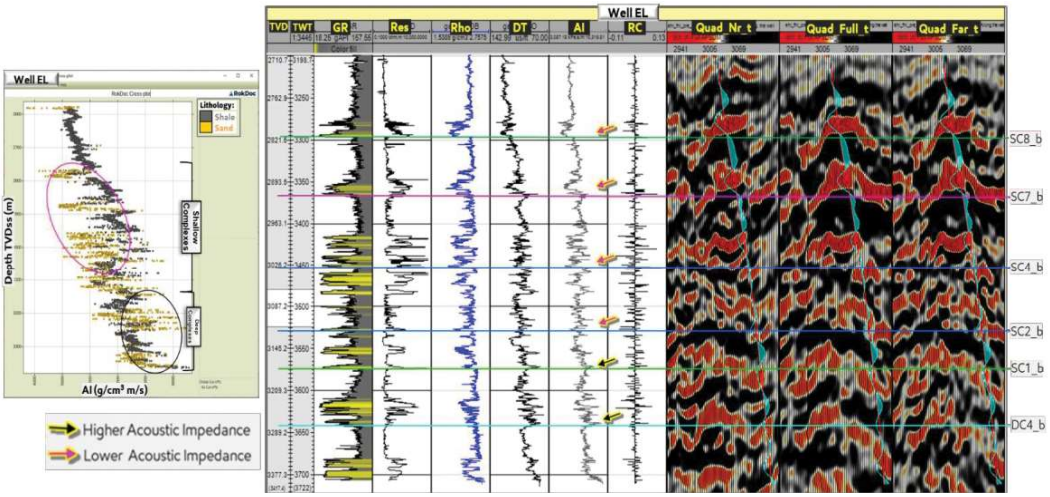

Figure 13: Well EL well-to-seismic tie and AI-depth cross plot. Note AI signature of low impedance sands (SC4, SC6 and SC8) vs high impedance sands (DC4 and SC1). Also observe cross plot and note that AI of sands is lower than surrounding overburden shales at shallow depths (Shallow channel complexes). The reverse is obtained at deeper intervals (Deep channel complexes).

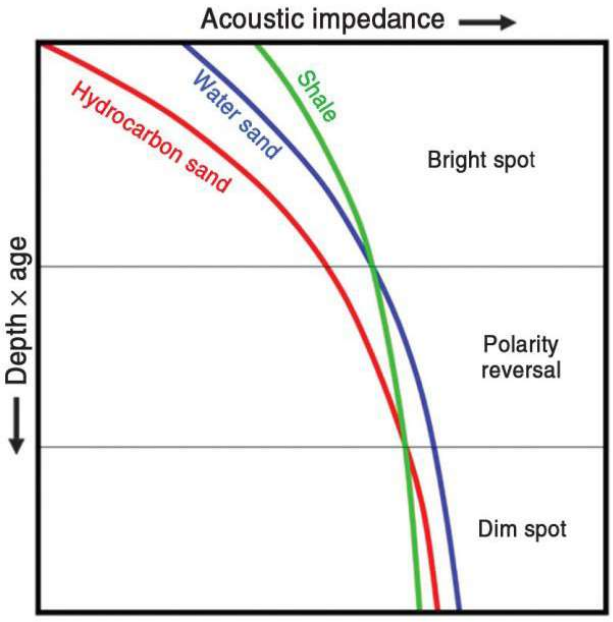

Figure 14: Brown and Abriel 2014 plot of acoustic impedance with dept and age showing normal compaction curves for sands and shales in same basin. Note the normal sequence of bright spot at shallow depths, polarity reversal at the transition or cross over zone, then dim spot at deeper intervals.

At well-by-well scale, the contrast in sand-shale acoustic impedance with depths is clearer as cross plots show better representation than those of figure 12b. The sands generally show lower acoustic impedance than shales at shallow depths but flip to higher values at deeper intervals (Fig. 15). This is similar to Vp – depth plot of figure 12d except that Vp for sands has similar range with shale at shallow depths but separates to greater values beyond 2700 m TVDSS depth range (equivalent of 1700m BML). So, we infer that both acoustic impedance and Vp-depth trend suggest that sandy rocks start off with slower velocities than surrounding shales at shallow depths where the sands are less compacted but become faster at deeper depths where they become more compacted than the shales. In Dada et al (2022), it is hinted that Vclay serves as a key input for accurate rock physics model and scatters in porosity-velocity relationships was attributed to lithology, especially to clay content. Other authors have related this to the dominance of mechanical compaction at shallow intervals where sands and shales have similar rates of porosity loss, but this changes at greater depths where cementation and chemical alteration have more impact on the shale mineralogy, thereby impacting their bulk property (Fig. 16). An analog to this field is the Paleogene deepwater complexes of Offshore Norway where Vp-depth trend show sands whose Vp at shallow depths is lower that surrounding shales but becomes higher at deeper intervals (Avseth, 2000) (Fig. 16). Transition zone of 1500m for the Norway analog compares closely with 1700m in this field. Although this cross-over depth may vary slightly from field to field, it represents the separation between the shallow placed zone of mechanical compaction and the deep-seated zone of cementation and chemical alteration (Avseth 2000; 2008). On the question of differential compaction between sands and shales, the platy clay fabric in the shales is more prone to compaction than the assemblage of non-platy, angular to sub- angular, or spherical shaped grains in sands; hence, the more rapid mechanical porosity reduction in shales than sands (Avseth *et al* 2008).

Our comparison between density, Vp, and AI trends, shows that the acoustic impedance is primarily impacted by Vp. It was observed that the AI log tracked Vp very closely and showed a very good match with the velocity log in most reservoirs while different from the density log (Figures 5, 6, 10 and 11). Hence, more research was done on Vp logs and possible controls on Vp trend. According to Han *et al.* (1986), Vp is a linear function of both porosity and clay content, decreasing as the porosity/clay content increases. Marion *et al.,* (1992) however, noticed an initial increase because of porosity reduction from clay particles filling spaces between sand grains. After a critical value, the Vp then decreased with clay content.

On Vp/Vs vs depth plot, Vp/Vs slightly decreases with depth even though the trend isn't quite as stark. Laboratory investigations by Tatham 1982 suggest that there is a relationship between the ratio of compressional to shear wave velocity (Vp/Vs) with lithology type. In other words, Vp/Vs is used as a lithology discriminator (sand vs shale). Vp/Vs for sands ranges between 1.5 to 2.2 while that of shales range from 1.8 to 2.4 (Fig. 12e and 17).

Propagating Interpretations away from well locations

Following successful delineation of both shallow and deep channel boundaries using integrated understanding from well points, the next step was utilizing Joint Impedance and Facies Inversion (JIFI) volumes to influence the 3D propagation of interpretations. Inversion input was primarily seismic angle stacks, rock property parameters, rock physics trends from calibration wells, and algorithms. The volume of sand and sand probability volumes were among key JIFI volumes used for guiding interpretations on the primary seismic interpretation volume. With this approach, there is high confidence in interpretations made and the challenge of vertical or lateral variation in observed acoustic impedance was significantly minimized.

In figure 19, there are pink boxes highlighting sample shallow channel sands (SC4 and SC7) at the wells. Note that the emphasized sand bodies correspond to troughs (negative values which represent low impedance intervals in this normal polarity quadrature data). These shallow sands are low acoustic impedance relative to surrounding

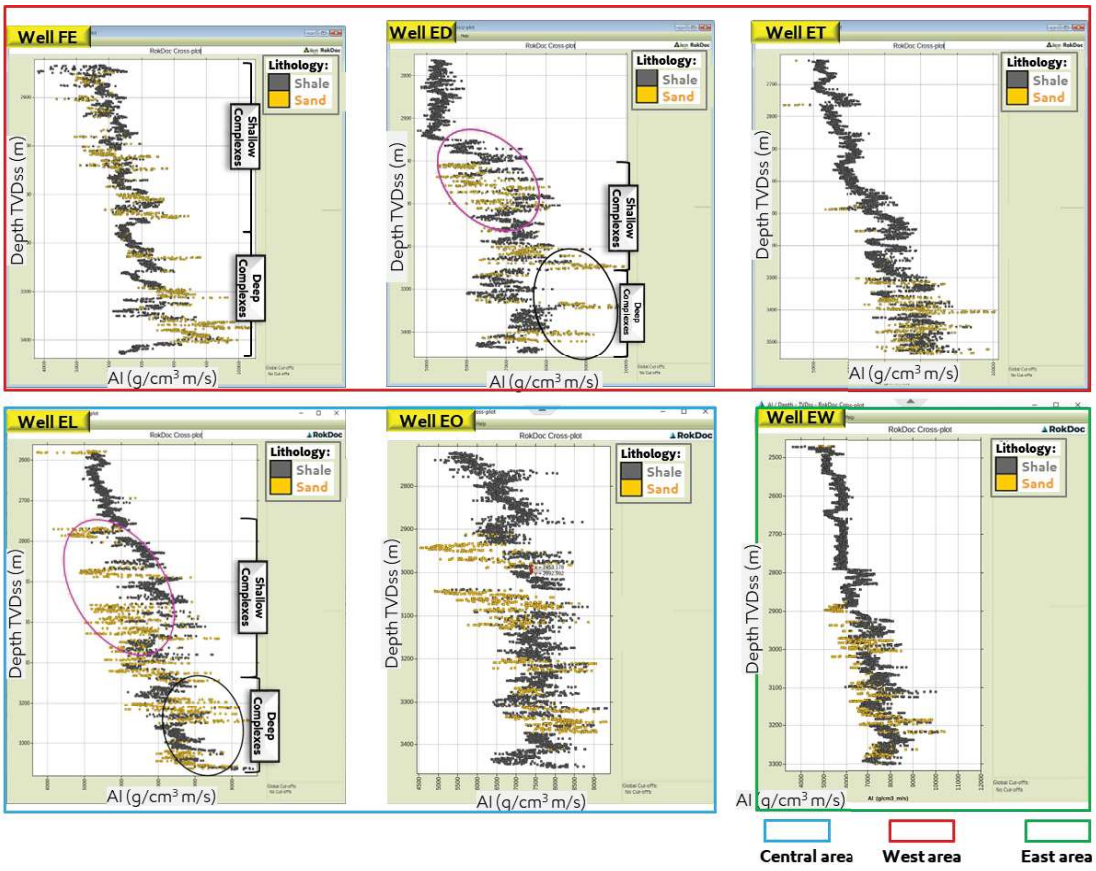

Figure 15: Sand and shale acoustic impedance for selected wells of study area. Note lower AI for sands than overburden shales at shallow depths (pink circles) followed by flips to higher AI at deeper intervals (black circles).

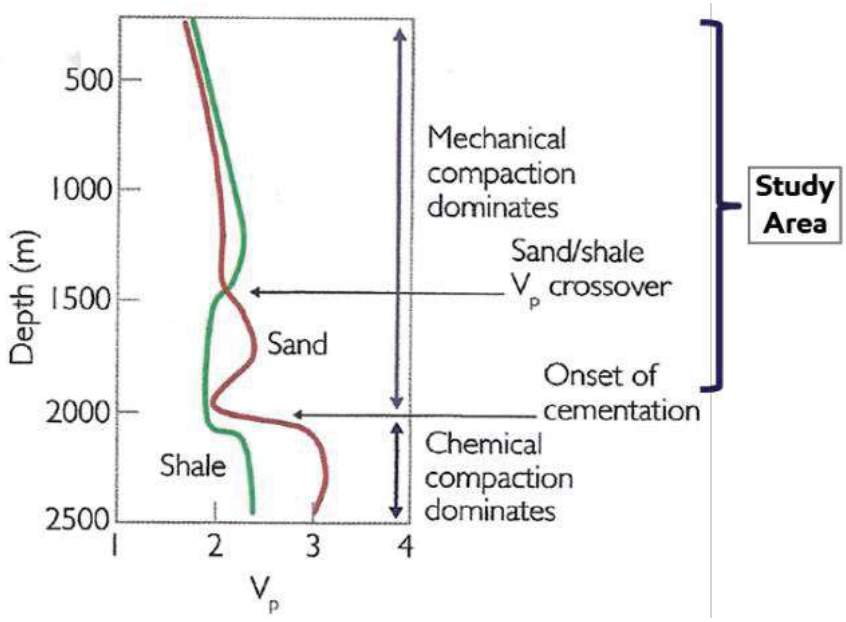

Figure 16: Generalized velocity-depth trends for sands and shales in the Paleogene offshore Norway (modified after Avseth, 2000).

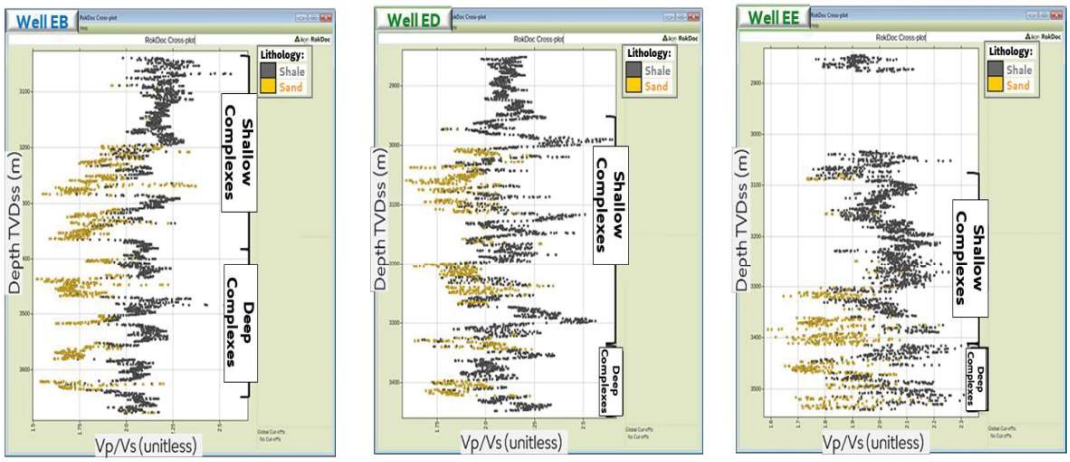

Figure 17: Vp/Vs vs depth plot for sand and shale rocks for wells EB, ED and EE. Note Vp/Vs for sands ranges between 1.5 to 2.2 while that of shales range from 1.8 to 2.4.

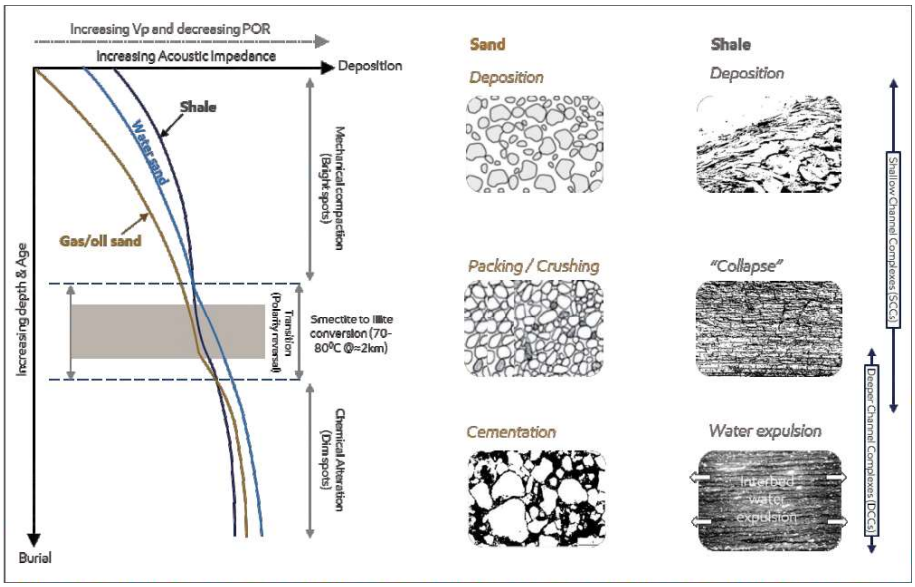

Figure 18: Generalized plots showing acoustic impedance, Vp and porosity trends with depth for sands and shale in study area. Note difference in impact of deposition burial on sands and shales. Also, observe progression from mechanical to chemical compaction zones in relation to shallow and deep channel complexes (modified after Brown and Abriel 2014; Avseth 2000).

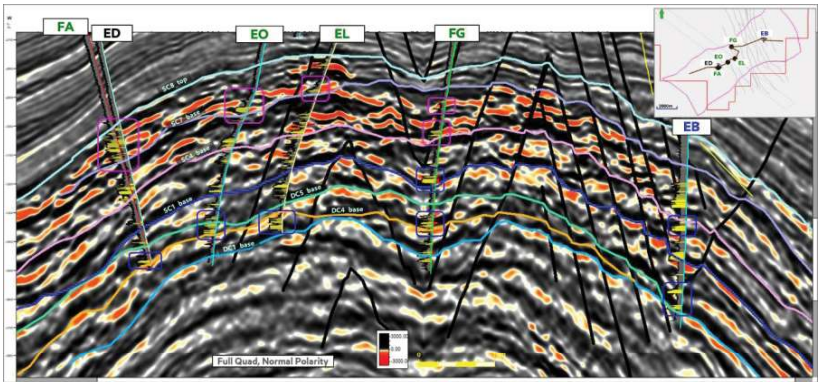

Figure 19: Note placement of channel base for selected Shallow and Deep Channel Complexes

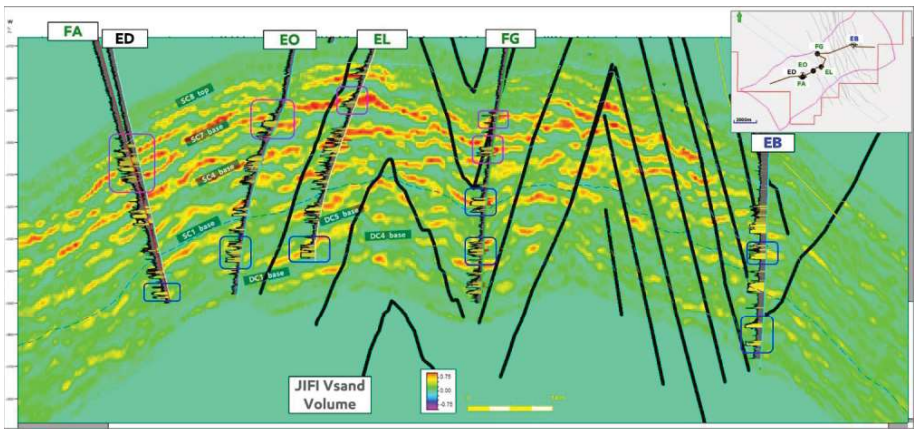

Figure 20: JIFI Vsand volume influenced 3D propagation for both low and high impedance sands, as well as mixed zones with low impedance contrast.

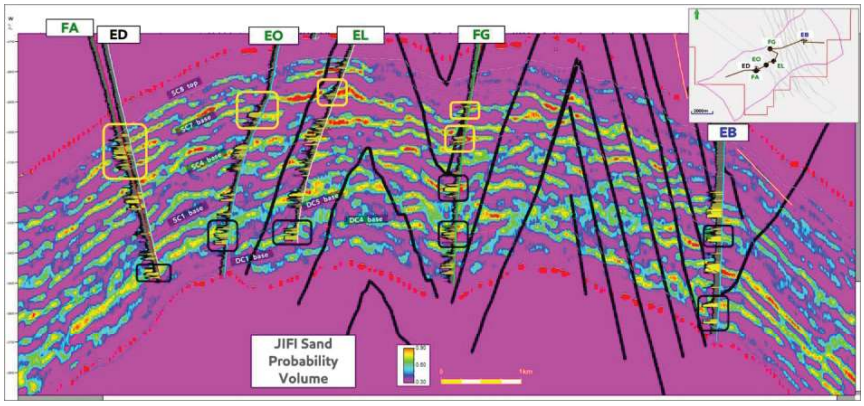

Figure 21: Note placement of channel base for selected Shallow and Deep Channel Complexes. JIFI Sand Probability influenced 3D propagation for both low and high impedance sands, as well as mixed impedance zones.

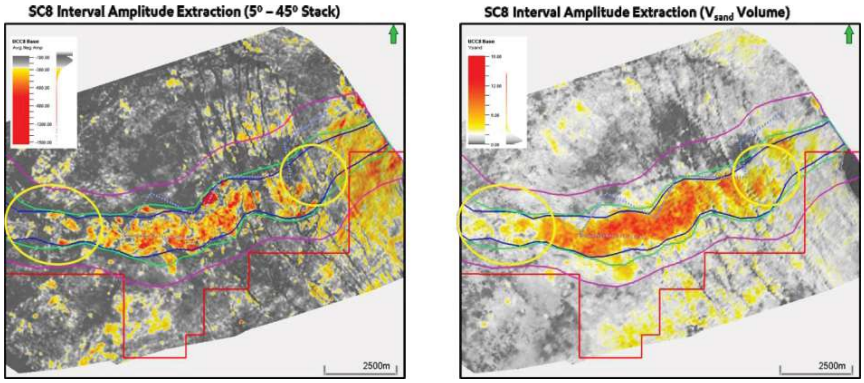

Figure 22: 3D Propagation: Observe yellow circles highlighting areas where JIFI inversion volume (figure 22b) shows improved reservoir fairway definition compared to the primary full stack seismic data (figure 22a).

shales. Also note that the base of the low impedance shallow channels tie to the trough to peak zero crossing. The deeper channel sands highlighted in blue boxes (DC4, DC5 and SC1) show the opposite character. In these deeper intervals, the sand bodies tie to seismic peaks (positive values representing high impedance sands) while the basal boundaries correspond to peak to trough zero crossing. Figure 20 and 21 showing the JIFI Vsand and sand probability volumes respectively, enabled QC and 3D propagation of interpreted framework horizons. This helped minimize uncertainties as both high and low impedance sands appear as same character on these

inversion volumes. These volumes also provided interpretation guide in transition zones where impedance contrast between sands and shales were either too low or where the sand flips from one impedance behavior to the other. The JIFI volumes also helped in definition of the overall sand fairway. Areas with ambiguous or poor amplitude patterns maps generated from the primary volume, were better defined when same fairway map was generated using the inversion volume as input (Fig. 22a and 22b).

SUMMARY AND CONCLUSION

In this investigation, thorough look at geological and rock physics parameters of Miocene deep water turbidites revealed that Acoustic Impedance (AI) in this study area is variable especially in the vertical sense. Sands of the shallow channel complexes mostly indicate low AI relative to surrounding shales while those of deeper channel complexes are mostly high AI. Seven genetic turbidite facies defined were defined through core-log integration and using Bouma's 1962 low energy turbidites and Lowe's 1982 traction high energy turbidites. Of the 7 genetic turbidites, the sandy rocks contain mostly R, S and Ta beds while the shaly rocks are dominated by Td and Te beds. It is observed that both low and high impedance sands contain similar turbidite facies, mostly R, S, Ta and Tb beds. However, there is concentration of bedload R and S beds in the high impedance sands. In the plots of bulk density against depth, sands containing high concentration Ta and Tb turbidites had lower density than those dominated by suspension turbidites namely Td and Te beds. Compressional velocity (Vp) vs depth plots reveal that sands containing mostly Td and Te beds have lower Vp range while R, S and Ta dominated sands are in the higher Vp spectrum. The acoustic impedance versus depth plot demonstrates that at shallow depths, there is significant overlap between Ta, Tb- dominated sands and Td, Te dominated sands. At deeper intervals, both Td and Te beds have lower impedance than Ta, R and S beds.

With respect to the fluid substitution modeling, the objective was to gain insights on expected AVO response at different fluid content, as well as check possible relationship between fluid type and observed acoustic impedance. Several sands showed a Class 2P response with the 2P occurring at progressively lower angle between in situ and gas fluid contents. We note that irrespective of fluid type (gas, oil or brine), the acoustic impedance of the sands (relative to shale) is not driven by fluid type as both high and low impedance sands show similar response in different fluid cases.

Cross plots of Vp, Vp/Vs, Den, Porosity and AI with Depth showed that density, AI, and Vp increases with depth for both sand and shale lithologies. However, most sands had lower AI than that of surrounding shales at the shallow depths but transition to higher AI than the shales at deeper intervals. This behavior, as hinted by several authors, is because sands and shales have different compaction trends. The Vp – depth plot reveals that Vp for sands has similar range with shale at shallow depths but separates to greater values beyond 2700 m TVDSS depth range (equivalent of 1700m BML). Both AI and Vp vs depth plots suggest that sandy rocks start off with slower velocities than surrounding shales at shallow depths where the sands are less compacted but becomes faster at deeper depths where they become more compacted than the shales. In all of Vp, porosity and acoustic impedance versus depth profiles, several authors have delineated three zones: A shallower zone dominated by mechanical compaction, where sands have lower AI than surrounding shales and bright spots are commonly identified. Following this is a transition zone, typically around 2km below seabed where polarity plots occur and impedance contrast between sands and shales can be quite minimal. The 70-800C depth within the transition zone marks onset of chemical alteration and where smectite to illite conversion is prevalent.

On closer look at the synthetic seismogram, it is observed that Vp (rather than density) has stronger control on the AI. This deduction is based on observation that the AI log tracked Vp very closely in most sands and showed minimal character match with the density log on the panel. The Vp/Vs vs depth plot showed separation between sand and shales with some overlaps recorded in a few wells. As is common knowledge, the Vp/Vs log plays the traditional role of lithology and rock facies discrimination. Observed Vp/Vs ranges is 1.5 to 2.2 for sands, while that of shales range from 1.8 to 2.4.

Summarily, fluid substitution and genetic DW lithofacies evaluation show minimal control on observed AI while burial depth (compaction) shows stronger impact on the reservoir Ais.

REFERENCES CITED

Abreu V., Sullivan M., Pirmez C., and Mohrig D., (2003). Lateral accretion packages (LAPs): An Important reservoir element in deep water sinuous channels. Marine and Petroleum Geology. Vol.20. Issues 6-8. P. 631 – 648. Https://doi.org/10.1016/j.marpetgeo.2003.08.003.

Al-khazraji O. N. A., Idan R. M., Salih A. L. M., Hassein R. K., (2018), Quantitative Implementation of Acoustic Impedance Inversion to Porosity and Lithology Prediction of Clastic Reservoir, Luhais Oil Field, Southern Iraq, Civil and Environmental Research, v.10, (6). ISSN 2224-5790 (Paper); 2225-0514 (online), p.10-18.

Andreassen K., Nilssen E. G., Ødegaard C. M., (2007), Analysis of shallow gas and fluid migration within the Plio-Pleistocene sedimentary succession of the SW Barents Sea continental margin using 3D seismic data, Geo-Mar. Lett., 27 (2007), pp. 155-171. DOI: 10.1007/s00367-007-0071-5.

Avbovbo, A.A., (1978), Tertiary lithostratigraphy of the Niger Delta: AAPG Bulletin, v. 62, p. 295-300.

Avseth P., Draege A., Johansen T. A., Wijngaarden A. V., and Jorstad A.,

(2008), Shale Rock Physics and Implications for AVO analysis: A North Sea Demonstration, The Leading Edge (TLE), June 2008, p.788-797. DOI: 10.1190/1.2944164.

Avseth P., Flesche H., and Wijngaarden A. V., (2003), AVO classification of lithology and pore fluids constrained by rock physics depth trends, The Leading Edge (TLE), October 2003, p.1004-1011.

Avseth P., (2000), Combining Rock Physics and Sedimentology for Seismic Reservoir Characterization of North Sea Turbidite Systems, PhD Thesis (Unpublished), Stanford University, California USA, 200pp.

Bjorlykke K., (1998), Clay mineral diagenesis in sedimentary basins—A key to the prediction of rock properties; examples from the North Sea Basin, Clay Minerals, v. 33, p. 15-34.

Bouma, Arnold H. (1962). Sedimentology of some Flysch deposits: A graphic approach to facies interpretation. Elsevier. p. 168.

Brown, A. R., Abriel W. L., (2014), Detection of hydrocarbons using non-bright-spot seismic techniques, Interpretation, Vol. 2, No. 4 (November 2014); p. SP1–SP4. https://doi.org/10.1190/INT-2014-0138.1

Corredor F., Shaw, J. H. and Bilotto, F., (2005). Structural styles in the deep-water fold and thrust belts of the Niger Delta: AAPG Bulletin, v. 89, p. 753-780, doi: 10/1306.02170504074.

Dada R., Obi, I., Obere F., and Thomas-Ideh O., (2022)., An Innovative Approach to Vclay Analysis and Rock Property Characterization: An Example from the Erha Field, Offshore Niger Delta, Nigerian Association of Petroleum Explorationists (NAPE) Bulletin, 31 (2), November 2022. p.99-106.

Han D., Nur A and Morgan D. (1986). Effect of porosity and clay content on wave velocity in sandstones.

Lowe, D.R. (1982). "Sediment gravity flows: II. Depositional models with special reference to the deposits of high-density turbidity currents". Journal of Sedimentology, Society of Economic Paleontologists and Mineralogists: v. 52, p. 279-297.

Marion D., Nur A., Yin H. and Han D. (1992). Compressional velocity and porosity in sand clay mixtures.

Obi I.S. and Mode A.W. (2011). Geological controls on reservoir architecture and heterogeneity: Example from braided river deposits in SE Nigeria. Nigerian Association of Petroleum Explorationists Bulletin. V.23/2. Nov. 2011 (ISSN: 0794 – 0172), P. 72 – 87.

Obi I.S., Ezeagwuna C.A., and Popoola, O.W. (2018). Trap Styles and Polyphase Structural Deformation of Deepwater Sediments in Greater Triangular Bulge (GTB) Area, Eastern Niger Delta - Offshore West Africa. Nigerian Association of Petroleum Explorationists Bulletin. V.27 No 2 (September 2018) (ISSN 0794-0172) P. 29-36.

Oomkens E., (1967). Depositional sequences and sand distribution in a deltaic complex: Geol Mijnb., v.46. P. 265 -278.

Oomkens E., (1974). Lithofacies relations in the Quarternary Niger Delta complex: Sedimentology, v.21. P. 195 – 222.

Storvoll V., Bjørlykke K., Mondol N. H., (2005), Velocity-depth trends in Mesozoic and Cenozoic sediments from the Norwegian Shelf: AAPG Bulletin, v. 89, p. 359 – 381.

Tatham, R.H., (1982), Vp/Vs and Lithology, Geophysics, vol.47, No3, p.336-344. http://dx.doi.org/10.1190/1.1441339.